PCCP

Accepted Manuscript

ROYAL SOCIETY OF CHEMISTRY

www.rsc.org/pccp

Selective Adsorption of L-Serine Functional Groups on the Anatase TiO_2 (101) Surface in Benthic Microbial Fuel Cells

Yan-Ling Zhao[a,b*], Cui-Hong Wang[d], Ying Zhai[a], Rui-Qin Zhang[c] and Michel A. Van Hove[b]

[a]*Institute of Material Science and Engineering, Ocean University of China, 266100 Qingdao, China*

[b]*Institute of Computational and Theoretical Studies & Department of Physics, Hong Kong Baptist University, Hong Kong SAR, China*

[c]*Department of Physics and Materials Science, City University of Hong Kong, Hong Kong SAR, China*

[d]*School of Science, Tianjin ChengJian University, 300384 Tianjin, China*

Abstract

To help design bacteria-friendly anodes for unmediated benthic microbial fuel cells (MFCs), we explore the role of anatase TiO_2 (101) surface biocompatibility in selecting functional groups of the levo-isomer serine (L-Ser), which contains carboxyl, hydroxyl, and amino groups in a single molecule. By performing total energy calculations and molecular dynamics simulations based on a density-functional tight-binding method, we find that at room temperature, the surface should be active for biomolecules with carboxyl/carboxylic and hydroxyl groups, but is not sensitive to those with amino groups. The hydrogen bonding between the hydroxyl H and surface O facilitates electron transfer from the pili or bacterial matrix to the anode surface, which improves the output power density. Thus, in combination with conductive polymers, anatase TiO_2 (101) surfaces can be an effective biocompatible substrate in benthic MFCs by enabling the surface O to form more hydrogen bonds with the hydroxyl H of the biomolecule.

Keywords: Anatase (101) surface; L-Ser; DFTB-D; explicit water environment

Introduction

Since microbial fuel cells (MFCs) have been proved to function well without additional mediators,[1-3] a large body of research[4-10] addresses the reuse of sewage sludge to produce electricity through this new technology. Reimers *et al.* report[10] that two benthic MFCs were deployed at a deep-ocean cold seep within Monterey Canyon, California, and were monitored for 125 days. Power records demonstrated a maximal sustained power density of 34 mW/m^2 of the graphite anode surface area. The low power density is the main limitation on the practical application of MFCs. One solution is to fabricate a more effective anode demonstrating high conductivity, high specific surface area, high porosity, noncorrosiveness, and low cost. With these requirements in mind, titanium dioxide (TiO_2) has been chosen as a component, codoped with polyaniline in anode materials[11-18] due to its biocompatible, stable, catalytic,[19] and nontoxic properties. As Qiao *et al.*[15] report, the nanostructured composite anode of TiO_2 with 30 wt % polyaniline delivers much higher power density (1495 mW/m^2) in *Escherichia coli* (*E. coli*) MFCs. Nevertheless, they use 5 mM 2-hydroxyl-1,4-naphthoquinone as the mediator to accelerate the electron transfer rate. In observation using SEM pictures, the pili were produced by the *E. coli* cells and jointly attached to the electrode surface to form a cross-linked network. TiO_2 played an important role in accelerating the electron transfer by promoting cell adhesion to the anode. Combined with the high conductivity of the polyaniline, the nanostructured polyaniline/TiO_2 composite demonstrated improved bio- and electrocatalytic performances in MFCs. However, the interaction mechanism at the molecular level is still far from clear, hindering the exploration of highly effective and "green" MFCs without pollutant mediators. It is thus desirable to know how the pili or bacteria matrix interact with the TiO_2 surface, how the aqueous environment affects the adsorption, and the pathway of the electron transfer. In this paper, we mainly focus on the biocompatible performance of TiO_2 in benthic MFCs to explore the interaction of the biomolecules with TiO_2 based on calculations at the quantum mechanical (QM) level to give theoretical support to the modification of anode materials.

The carboxyl (–COOH), amino ($–NH_2$), and hydroxyl (–OH) groups are common active groups within biomolecules. For instance, the bacterial cell wall[20] mainly consists of peptidoglycan with the backbone of the N-acetylmuramic acid and the N-acetylglucosamine alternately connected via the β-1,4 glycosidic bonds. The multilayered backbones are linked via the tetrapeptide stem of L-Alanine, D-Glutamic acid, meso-2,6-diaminopimelic acid, and D-Alanine for Gram negative, or L-Alanine, D-Glutamine, L-Lysine, and D-Alanine for Gram positive with an additional pentaglycine interpeptide bridge. These structures are too complicated to calculate using *ab initio* methods. Even the molecular weight of 3048 of the pilus of *E. coli*[21]

reaches 17,000 with a radius 5 to 7 nm. In carrying out fundamental theoretical studies, amino acid monomers or analogues have frequently been chosen as representatives of bioorganic systems to study their interactions with inorganic surfaces.[22-26] In this way, functional group adsorption can be clearly categorized and summarized in terms of favorable configurations, binding energies, and electron transfer characteristics, so as to guide the modification of materials for anchoring the target biomolecules. To date, many researchers have studied the interaction of amino acid or analogues with titania surfaces both experimentally and theoretically.[23,27-40] Most have concluded that the carboxyl moiety is more favorable than the amino group on TiO_2. As revealed by X-ray photoelectron spectroscopies,[28,31] titania shows a much great affinity for the carboxyl group and are chemically reactive only in an acidic environment. No agreement has been reached on the carboxyl preferred binding state on the surface. Gong *et al.*[33] point out that formic acid is spontaneously deprotonated on the anatase (001) surface, based on density functional theory (DFT) calculations and molecular dynamics (MD) simulations. The bidentate adsorption configurations, in which the formate moiety binds to the surface through two O-Ti bonds, are more favored energetically than monodentate configurations. In contrast, Vittadini *et al.*[29] and Nilsing *et al.*[32] both report that on the surface of clean anatase (101) the most stable adsorption structure for the formic acid is a molecular monodentate configuration, with hydrogen bonded to a surface bridging O. The different binding states may come from the distinct surface patterns, but the mechanism of the proton transfer from the molecule to the surface is still uncertain. Szieberth *et al.*[36] report, based on a DFT study, that the glycine molecule could bind to the anatase (101) surface in its most stable configuration, utilizing both the carboxyl and the amino groups without proton dissociation. This implies that the amino acid could sustain its proton in its neutral molecule and the amino group could bind with the surface through an N-Ti bond. Substantial N-Ti interactions[37-39] have also been found in other work examining NH_3 gas and the anatase (101) surface through spin-polarized[37,39] DFT calculations. The results in relation to N-Ti interaction seem questionable as they have not been confirmed experimentally.[28,31] We ascribe this discrepancy to the difference in research conditions. As a photocatalyst, TiO_2 demonstrates high reactivity to external species by gaining energy from sunlight radiation or heat.[30] In the ground state, stoichiometric TiO_2 surfaces might be very inert to NH_x species. As for the –OH, few studies have elaborated the adsorption behaviors of the hydroxyl group on the surface. A very early study by Kim *et al.*[27] investigates the adsorption of aliphatic alcohols on anatase powders and shows that the molecular alcohols desorbed intact on the slight application of heat (at 350 K). A recent theoretical work[23] confirms that there may be some potential for methanol to hydrogen bond to the titania surface.

It is thus necessary to clarify the binding configurations of the carboxyl, amino,

and hydroxyl groups on TiO_2 in benthic MFCs. The aqueous effect on the adsorption configurations also needs to be studied to simulate the actual environment for practical applications. However, this presents a great challenge due to the huge computational costs involved. In this paper, we focus on the levo-isomer serine (L-Ser) since it contains three active groups in one unit. Firstly, we compare the ability of the three moieties (–COOH/COO^-, –OH, and –NH_2/NH_3^+ groups) to attach to titania surfaces. Then, we look at how, as a simplified biomolecule, the L-Ser enables reduced computational time to be used in QM calculations when an explicit water environment is introduced into the calculations.

Computational details

The density-functional tight-binding method complemented by a dispersion term (DFTB-D) in the total energy is a highly efficient semi-empirical method which can handle large models at a reasonable computational cost while retaining a level of accuracy comparable to DFT. It was developed on the basis of a tight-binding model, which assumes that the bulk electrons are tightly localized in atomic orbitals which are then combined linearly to represent the electron orbitals of the solid.[41-45]

Previous studies validate the reliability of DFTB-D for describing the interactions between amino acids and inorganic materials.[46-48] In particular, it has been proved that DFTB gives qualitative consistency for the adsorption of molecules (phosphonic acid,[49] benzene,[50] acetic acid,[51]) on TiO_2 in comparison with DFT or experimental results. In this work, we used the DFTB-D method (version 1.2[44]) to study the L-Ser attachment on titania surfaces with the long-range interaction included as a Lennard-Jones functional described by universal force field parameters. The complexes were optimized using a conjugated gradient algorithm. The charge convergence criterion was set at 10^{-5} electrons. All the Slater-Koster parameters involved in the atomic pairs are available at http://www.dftb.org and obtained from the directories tiorg-0-1 and mio-0-1. Spin polarization is not considered here since TiO_2 plays the role of biocompatible substrate in a stable state.

To go beyond static calculations so as to draw more convincing conclusions and ensure the stabilities of the structures screened out by optimizations, we also performed DFTB-D-based MD (DFTB-D/MD) simulations for a period of 10ps to track the adsorption stabilities of the three functional groups on the surface. We used the canonical ensemble with Anderson thermostat in an NVT model. Considering that the temperature of actual seawater usually varies from 0 to 30 °C, depending on vertical depth and season, and that in laboratory testing the benthic MFCs devices are normally kept at room temperature, the thermostat was set to T = 300 K with a time step of 1 fs for the integration of the equations of motion, which were resolved using a

Verlet velocity algorithm.

Structural model

In this work, we modeled a stoichiometric titania surface without hydroxylation. A hydroxylated TiO_2 surface is usually induced by surface defects[52] and has high chemical reactivity, leading to water or amino acid dissociation.[53] We certainly do not expect TiO_2 to play a sterilization role in benthic MFCs, which rely on live bacteria permanently eating organic matter and releasing electrons to the anode. Furthermore, the pH value of seawater ranges from 7.5 to 8.3,[10] providing a stable basic environment for TiO_2 surfaces without chemical reactivity.

The anatase TiO_2 (101) surface was calculated by DFT study to have the smaller surface energy than that for the rutile phase.[54,55] In spite of the experimental fact that rutile is thermodynamically most stable, with slight advantage, we are still interested in selecting the anatase (101) as the surface model in our study because it is less studied but often mixed with rutile in the commercial TiO_2 powder. Periodic boundary conditions were used with a unit cell defined by a=20.4 Å, b=15.1 Å, c=30.0 Å, and $\alpha=\beta=\gamma=90°$. This ideal surface area is large enough to avoid interaction from adjacent copies of anchoring species. This slab surface is terminated by two-fold coordinated bridge O atoms and five-fold coordinated Ti atoms as well as three-fold coordinated O atoms. It is 6 layers thick, containing 96 Ti and 176 O atoms. Along the c axis, the cell dimension was set to be 21 Å to provide sufficient vacuum thickness between the repeated slabs.

In order to take the water environment into account, the remaining space within the box was filled with 163 water molecules, which were randomly distributed and maintained the density of the solution at 1.0g/cm^3. The random distribution of water molecules was automatically generated using the Gromacs package[56] by checking the overlaps of the Coulomb and VdW radii. The anatase (101) surface in water solution mainly undergoes water adsorption without dissociation, as shown by experimental IR[57] and XPS measurements[58] and a previous DFT calculation.[59]

Since only the levo (left-handed) isomer of amino acids is found in living creatures, L-Ser was used. In a water solution, neutral L-Ser will automatically become zwitterionic. For simplicity, we denote the hydroxyl O and H atoms of the carboxyl group as O1 and H(–COOH) or H^+(–COOH), the double-bond carboxyl O as O2, the side chain hydroxyl O and H atoms as O(–OH) and H(–OH), and the amino N and H atoms as N($–NH_2$) and H($–NH_2$) or H^+($–NH_3^+$), respectively. The O and Ti atoms on the surface are each designated as O_{surf} and Ti_{surf}.

Results and discussion

1. Energetics of adsorption

By attempting the –COOH, –OH, or $–NH_2$ moieties of the neutral L-Ser approaching the clean anatase (101) surface, five adsorption geometries are ultimately confirmed, denoted by S1, S2, S3, S4, and S5 and ordered by increasing total energy (E_{tot}); in other words, decreasing stability. As illustrated in Figs.1 (a)-(e), in Sn for n = 1 to 4, the neutral L-Ser prefers releasing the proton of the –COOH to the surface and forming an O–Ti bond through the carboxyl O2 with the Ti_{surf} in lengths of 2.012, 1.986, 1.993, and 1.983 Å, respectively. As listed in Table 1, critical interatomic distances are labeled with the same numbers shown in Fig. 1. The proton is covalently bonded to the O_{surf} and simultaneously forms a hydrogen bond with the carboxyl O1 in the configuration of [O_{surf}–H^+…O1], with O_{surf}–H^+ distances of 0.989, 1.005, 0.993, 0.992 Å, and H^+…O1 distances of 1.820, 1.669, 1.735, 1.765 Å. The monodentate immobilization of the carboxyl species on the surface induces a bond-type conversion in the $–COO^-$. The length of the original double bond between the carboxyl C and O2 in Sn for n = 1 to 4 is enlarged to 1.328, 1.305, 1.308, and 1.323 Å, but is still shorter than the C-O single bond length of 1.380 Å in a single L-Ser molecule. The length of the original single bond between the carboxyl C and O1 is decreased to 1.245, 1.253, 1.253, and 1.248 Å, but is still longer than the 1.218 Å of the C=O double bond in L-Ser. Hence, there exists π electron conjugation in the $–COO^-$ due to the formation of an O-Ti bond with the surface.

In S1, S2, and S4, the H(–OH) of the L-Ser prefers to hydrogen bond with the O_{surf} with H(–OH)…O_{surf} distances of 2.010, 1.858, and 1.758 Å. In S1 and S3, the O(–OH) approaches the Ti_{surf} at distances of 2.152 and 2.160 Å, which are only about 8% longer than the bulk O-Ti bond length (~2.0 Å).[60] Since the O atom carries a negative and Ti atom a positive charge, at such short distances electrostatic attraction is probably generated. Such interactions cannot be neglected as they may play an important role in determining the favorable orientation of biomolecules on metal oxide surfaces. Interestingly, both Coulomb attraction and hydrogen bonding can coexist when the –OH matches well with the surface, as identified in S1.

In S1 and S3, the H($–NH_2$) forms hydrogen bonds with the O_{surf} at distances of 2.008 and 1.952/2.158 Å (two for S3). In S5, the H($–NH_2$) and the H(–COOH) simultaneously form hydrogen bonds with the O_{surf} at distances of 2.042 and 1.700 Å. Notably, no proton transfer occurs in S5, implying the possible molecular adsorption of the L-Ser on the surface.

As listed in Table 2, the E_{ads} values of S1 to S4 are -46.15, -43.77, -42.18, and -39.15 kcal/mol, respectively. In S1 and S4, the $–COO^-$ and the proton interact with

the adjacent Ti_{surf} and O_{surf} atoms, namely the top site, while in S2 and S3, they are bonded to the separated atoms, namely the hollow site. Judging from the values of E_{ads}, there seems to be no obvious relationship between the L-Ser favorable adsorption and the surface sites. However, the surface morphology indeed influences the L-Ser attachment by way of the diverse conformations shown in S1 to S5. The L-Ser attempts to interact with the two-fold coordinated O_{surf} and five-fold coordinated Ti_{surf}, by releasing the proton and forming an O-Ti bond, and generating hydrogen bonds and/or Coulomb attractions. In this way, the total energy is significantly lowered and the stability of the complex is much improved.

However, strain energy (E_{strain}) in the L-Ser is also generated, since the L-Ser must distort itself to bind with the surface. The total energy lowered by the adsorption of the functional groups is partially counteracted by this strain energy. To describe this, we calculated the energy difference between the single point energy of the deprotonated L-Ser in Sn for n= 1 to 4 and a free deprotonated L-Ser, and the energy difference between the single point energy of the L-Ser in S5 and an isolated L-Ser molecule. Although three functional groups of the L-Ser in S1 all interact effectively with the surface, E_{ads} is only slightly lower than that of the other conformers. One reason for this is that the total energy is lifted by the strain energy of 14.35 kcal/mol. In S3, the strain energy reaches as high as 17.30 kcal/mol. By contrast, the strain energy for S5 is only 2.07 kcal/mol. This is because the L-Ser matches the surface well in this configuration. Thus, effective adsorption is not only related to the activity of two parties but also to how well they match. Furthermore, the deprotonation is induced by surface morphology, but not spontaneously given by the –COOH, as shown in the molecular adsorption in S5. That is why the amino acid has ever been found to be adsorbed on the TiO_2 surface in a molecular or deprotonated form. Nonetheless, the L-Ser molecular adsorption is not as favorable as for the deprotonated case due to S5 showing the smallest E_{ads} at -19.71 kcal/mol.

Although an O-Ti bond was formed in Sn for n= 1 to 4, their E_{ads} was only around -40 kcal/mol. Since the [O-H…O] hydrogen bond energy is usually about -10 kcal/mol,[61,62] and considering both the strain energy in the L-Ser and Coulomb attraction, we estimate the O-Ti binding energy as about -30 kcal/mol, which is a relatively weak O-Ti interaction. Nonetheless, sunlight does not penetrate the sea floor. This stable environment for benthic MFCs basically assures the irreversible $–COO^-$ immobilizations of bacteria or pili on the TiO_2 surface.

The E_{ads} results confirm that there is a definite Coulomb attraction between the O(–OH) and the Ti_{surf}, since S3 with an extra Coulomb interaction is more stable than S4. Moreover, such an interaction could even reduce the strength of the hydrogen bond. When the L-Ser adjusts its –OH orientation on the surface and generates a Coulomb attraction, the ideal interacting direction for forming hydrogen bonds will be

partly changed. By comparing the data in Table 2, we conclude that the O(–OH)…Ti_{surf} Coulomb binding energy is comparable with the H(–OH)…O_{surf} hydrogen bonding in the range -5 to -10 kcal/mol.

The N(–NH_2) could, in principle, interact electrostatically with the Ti_{surf}, but we found no adsorption geometries with a N…Ti_{surf} distance less than 3 Å. When the N with its lone pair of electrons gets close to the Ti_{surf}, a coordination bond may form between them. We ever attempted with placing the N of an NH_3 molecule with the Ti_{surf} of the anatase (101) surface. It turns out the Ti-N distance is equilibrated at 2.458 Å, which is about 16% longer than the covalent bond length 2.12 Å[63] in the TiN crystal. This indicates that this Ti-N bond is weak and easily broken. In reality, the group –NH_2 from biomolecules generates larger steric hindrance than an isolated NH_3 and so barely overlaps with the 3d orbitals of Ti_{surf} along an optimal direction. This is why we found no N-Ti adsorption geometries. Unlike N(–NH_2), the single carboxylic O has no problems of steric hindrance and easily forms an ionic bond with the Ti_{surf}, which again shifts to its six-coordinated form. At the same time the –COO^- rearranges its electron distribution by changing the original double bond to a single bond. Considering all the results from our static calculations in vacuum, we propose that the preferential adsorption order for the three functional groups is –COOH, –OH, and –NH_2, from strongest to weakest. However, this contention requires further support from MD simulations and these are presented in the next section.

2. Dynamics of the adsorption systems

We undertook further study of the five systems defined above using DFTB-D/MD simulations in vacuum for 10ps. We aimed to observe the attachment stability of the functional groups on the surface without the impact of water. In benthic MFCs, the anode is embedded in marine sediment which has a lower water content than seawater. It is likely that some biomolecules on local areas of the porous titania surface would be immobilized in an anhydrous or water-scarce environment.

As shown in Table 3, in the final 3ps, the root mean square deviations (RMSD) of the temperature is 14 to 15 K and the RMSD of the total energy is 17 to 18 kcal/mol. Thus, we can assume that the system has reached equilibrium at this stage.

As illustrated in Figs. 1 (f)-(j), the MD configurations in vacuum at the final time step are denoted as Sn_{vac} for n= 1 to 4, which are basically similar to the static geometries of S1 to S4. Surprisingly, the molecular adsorption in $S5_{vac}$ is retained, but the hydrogen bond of H(–NH_2)…O_{surf} vanishes. This reflects the instability of the thermal adsorption of the –NH_2 on titania, contrasting with the stable adsorptions of the –COOH and –OH groups.

To identify the orientation of the L-Ser on the surface, we examined the time

evolution of critical distances, as depicted in Figs. 2-4. Firstly, the distances between O2 and Ti_{surf} in Sn_{vac} for n = 1 to 4 all fluctuate constantly as a function of time, as shown in Fig. 2 (a). As summarized in Table 4, their average O-Ti bond lengths in the last 3ps are 1.980, 1.963, 1.998, and 1.950 Å with RMSD in the range 0.043 to 0.053 Å. The distances between H^+(–COOH) and O_{surf} are all perfectly equilibrated at around 1.0 Å, as shown in Fig. 2 (b). Both indicate the formation of stable O-Ti and H-O bonds in vacuum. The distances between H^+(–COOH) and O1 illustrate that the hydrogen bonds are relatively stable due to the major distribution in the range 1.5 to 2.0 Å. The distances over 2 Å mean that the hydrogen bond is substantially affected as the L-Ser adjusts its favorable orientation on the surface, but ultimately well sustained. In $S5_{vac}$, the distance between H(–COOH) and O_{surf} mostly varies from 1.5 to 2.0 Å while the distance between H(–COOH) and O1 is stabilized at 1.0 Å, proving that the neutral L-Ser molecule can be sustained on the surface without deprotonation, at least in the first 10ps of the MD simulation. The distance between O2 and Ti_{surf} in $S5_{vac}$ fluctuates between 2.5 and 3.0 Å, demonstrating only a small Coulomb attraction between the –COOH and the surface.

The –OH group in Sn_{vac} for n= 1 to 4 also exhibits permanent adsorption via hydrogen bonds and/or Coulomb interactions, as shown in Figs. 3 (a) and (b). In $S1_{vac}$ and $S3_{vac}$, the distances between O(–OH) and Ti_{surf} are equilibrated at around 2.2 Å, reflecting the stable Coulomb attractions, while the H(–OH) and O_{surf} distances have larger fluctuations. This suggests that the hydrogen bond disappears as the values exceed 2 Å. The side chain –OH flexibly adjusts its position to preferentially interact with the surface through Coulomb attraction, leading to the vanishing of the hydrogen bonds. Under such conditions, Coulomb attraction is more favorable on the surface than hydrogen bonding. In $S2_{vac}$, the distance between H(–OH) and O_{surf} remains almost unchanged throughout the MD simulation. The distance between O(–OH) and Ti_{surf} varies slightly around 2.9 Å in the first 1.5ps, then drops toward a shorter distance at around 2.2 Å from 7 to 10ps, which we ascribe to the substantial Coulomb interaction generated between the O(–OH) and the Ti_{surf}. It indicates that the side chain –OH group could spontaneously match the local surface topology to form a stable attachment. In $S4_{vac}$, the –OH continuously and stably forms hydrogen bonds to the surface, while no Coulomb interaction is observed. This is due to the fact that the hydroxyl O atom is not initially pointed towards the surface and so has no chance to approach the Ti_{surf} in the first 10ps. The Coulomb attraction might appear over a longer simulation period. However, confirm that the –OH group of biomolecules is also active in attaching to the anatase (101) surface via hydrogen bonding and/or Coulomb interactions flexibly fitting the surface morphology.

Unfortunately, the $–NH_2$ group adsorption is insensitive to the surface. As shown in Table 1 and Fig. 4 (a), originally there are hydrogen bonds between H($–NH_2$) and

O_{surf} in S1, S3, and S5, but after 10ps the distances between H(–NH_2) and O_{surf} are all over 2.2 Å, indicating that these have disappeared. The distance between H(–NH_2) and O_{surf} undergoes strong fluctuations in $S5_{vac}$. This clearly demonstrates that the –NH_2 leaves the surface.

Our MD results in vacuum imply that the adsorption strength of the three groups is –COOH, –OH, and –NH_2 running from high to low. We find that the neutral –COOH of biomolecules can indeed attach to the surface, but the deprotonated state is energetically preferred, followed by immobilization on the surface via the O–Ti bond.

3. Solvent effects

Most MFCs function in an aqueous environment. Accordingly, we also performed the DFTB-D/MD simulations in solution for 10ps in order to explore the effect of water on the interaction between the functional groups and the titania. The starting configurations were still based on the static geometries of Sn for n = 1 to 5 but with the proton moved from the carboxyl to the amino side to generate a zwitterionic L-Ser (zL-Ser). The MD configurations in solution at the final time step are denoted as Sn_{sol} with n = 1 to 5. As shown in Table 3, in the final 3ps, the RMSD of the temperature was 8 to 10 K and the RMSD of the E_{tot} was 28 to 36 kcal/mol for Sn_{sol} for n = 1 to 4 and 105 kcal/mol for $S5_{sol}$. Due to a large change in the $S5_{sol}$ configuration, its total energy fluctuated substantially. We assume that the other systems Sn_{sol} for n = 1 to 4 reached equilibrium at this time.

As illustrated in Figs. 1 (k)-(o), the MD configurations at 10ps clearly exhibit a proton transfer from the –NH_3^+ to the O_{surf} in $S1_{sol}$, $S3_{sol}$ and $S5_{sol}$, but remains as –NH_3^+ in $S2_{sol}$ and $S4_{sol}$. No solvated protons are observed during any of the MD simulations, in agreement with the experimental fact that the amino acid is well stabilized in a zwitterionic form under aqueous conditions. In our previous study,[64] by SCC-DFTB static calculations and MD simulations for a zwitterionic glycine interacting with 310 water molecules, we also did not find any solvated protons even when nine hydrogen bonds were formed between the zwitterionic glycine and water.

The time evolution of critical distances in $S1_{sol}$ to $S5_{sol}$ is set out in Figs. 2-4. The distances between O2 and Ti_{surf} for Sn_{sol} with n = 1 to 4 are still well equilibrated, with average O-Ti bond lengths of 2.012, 1.995, 2.013, and 2.007 Å in the last 3ps, as seen in Table 4. Their average O-Ti bond lengths in solution are all longer than in vacuum. Although most of the O-Ti bond length fluctuations are larger than the bond length differences between vacuum and solution, it is still apparent that the water environment can elongate the O-Ti bonds and weaken, to some extent, the immobilization of the –COO^- group. As an illustration, the O-Ti bond length difference (0.057 Å) between $S4_{vac}$ and $S4_{sol}$ is longer than the RMSD values (0.043

Å in vacuum and 0.046 Å in solution). In $S5_{sol}$, the distance between O2 and Ti_{surf} reduces quickly to about 2.0 Å after 500 fs when the $–COO^-$ group comes into direct contact with the surface. This implies a high probability of the carboxylic attachment on the surface in the aqueous environment.

The –OH adsorption on the surface is also weakened to some extent by the solution. As shown in Fig. 3, the Coulomb interactions in $S1_{sol}$ and $S3_{sol}$ are very stable (as much as $S1_{vac}$ and $S3_{vac}$) during the whole MD simulation, but their hydrogen bonds fluctuate so strongly that they basically disappear over the entire 10ps. For $S3_{sol}$ in particular, the hydrogen bond is formed only in the first 1ps and then completely vanishes as the distance between H(–OH) and O_{surf} exceeds 4Å in the last 7ps. Unlike $S2_{vac}$, a Coulomb interaction in $S2_{sol}$ is not found systematically between the O(–OH) and Ti_{surf} but the hydrogen bond between H(–OH) and O_{surf} is still very stable. In $S4_{sol}$, the only hydrogen bond present is very stable across the whole MD simulation and is essentially similar to that of $S4_{vac}$. It is hard for the –OH of the zL-Ser to interact with the surface in solution using both hydrogen bonding and Coulomb interaction. This is because water can flexibly form hydrogen bonds with the zL-Ser so that the matching opportunity for the –OH on the surface is reduced.

Fig. 4(b) shows that the protons of the $–NH_3^+$ in $S1_{sol}$, $S3_{sol}$, and $S5_{sol}$ are released within 100fs, 3ps, and 2ps, respectively, and are covalently bonded with the O_{surf}, as shown by the enlarged distances between $H^+(–NH_3^+)$ and N and the reduced distances between $H^+(–NH_3^+)$ and O_{surf} (equilibrated at ~1Å). Most notably, the hydrogen bond is first randomly formed in the form of $[O_{surf}–H^+…N]$, but ultimately vanishes as the $–NH_2$ leaves the surface. It means that the $–NH_2$ attachment on the surface is still unfavorable in the water environment. In addition, the $–NH_3^+$ presents the same deprotonation behavior as the –COOH, due to the induced effect of surface morphology, as the $–NH_3^+$ of $S1_{sol}$ and $S4_{sol}$ are relatively far from the surface and do not release protons. Without proton transfer, the total energy of $S2_{sol}$ and $S4_{sol}$ is over 46 kcal/mol higher than with deprotonation ($S1_{sol}$ and $S3_{sol}$), as shown in Table 3. The $S5_{sol}$ is not discussed here because this system is far from well equilibrated.

Based on the results of these MD simulations in solution, we can infer that the three groups have the same attachment ability on the surface as in vacuum, with $–COO^-$, –OH, and $–NH_2$ in a decreasing sequence.

4. Mulliken charges

Charge distribution usually reflects the electron transfers in complexes. The Mulliken partial charges on relevant conformers and atoms were obtained from the DFTB-D/MD results in vacuum and solution and summarized in Table 5.

The original Mulliken charges of the surface and the L-Ser/zL-Ser are zero before

interaction. After adsorption in vacuum, the Mulliken charges on the deprotonated L-Ser in $S1_{vac}$ to $S4_{vac}$ at 10ps are -0.336, -0.303, -0.276, and -0.407 electrons, respectively. It can be seen that the interacting surface takes a positive charge with the same absolute value after the proton migration. This is highly unfavorable because the functioning anode surface requires electrons rather than positive charges from the biomolecules. In $S5_{vac}$, since a hydrogen bond remains in place between H(–COOH) and O_{surf} and L-Ser without losing a proton, the surface takes little negative charge with -0.036 electrons.

The electron transfer in solution is significantly different. The zL-Ser in $S2_{sol}$ and $S4_{sol}$ carries considerable positive charge with values of +0.337 and +0.293, respectively. This means that without deprotonation, the electrons are likely to be transferred from the zL-Ser to the surface. This is relatively favorable as we know that electron migration from bacteria to a surface will accelerate and improve the output power density of MFCs. However, in $S1_{sol}$, $S3_{sol}$, and $S5_{sol}$, the deprotonated L-Ser after adsorption takes a negative charge in each case, with values of -0.285, -0.325, and -0.470, respectively. The proton migration to the surface hinders the electron transfer from the L-Ser to the anode surface and should be avoided. Technically, a basic solution can help prevent proton binding with the surface as H^+ and OH^- show rapid neutralization in aqueous solution. Fortunately, in a benthic MFC, the weakly basic seawater provides a very promising environment for developing this technique further.

For comparison purposes, we also performed DFTB-D/MD simulations for 10ps as the clean anatase (101) surface in vacuum and 163 H_2O. The Ti_{surf} from a clean TiO_2 surface carries +0.871 e in vacuum and +0.853 e in solution and the O_{surf} takes -0.494 e in vacuum and -0.572 e in solution. Regardless of whether they are in vacuum or solution, for the O-Ti bonding and Coulomb interactions, the Ti atoms carry more positive charges than they did before adsorption as compared with the data in Table 5. Therefore, the O-Ti bond formation and Coulomb attraction cannot introduce electron transfer from the biomolecules to the surface, but only in the opposite direction. By contrast, in the hydrogen bonds between H(–OH) and O_{surf} from $S1_{vac}$, $S2_{vac}$, $S3_{vac}$, $S5_{vac}$, $S2_{sol}$, and $S4_{sol}$, the O_{surf} carries more negative charges than it did before adsorption. This means that the hydrogen bonds between the H(–OH) and the O_{surf} are the more favorable pathway for electron transfer from the biomolecules to the anode surface. This can also be shown by the interaction of water with the surface. As the water H could form a hydrogen bond with the O_{surf}, the surface ends up carrying more negative charge, with over -3 electrons in all configurations. The aqueous environment therefore greatly facilitates electron transfer from the water to the surface. This is a very promising tendency which cannot be found in vacuum. Therefore, to increase the output power density of MFCs, we

suggest choosing a hydrophilic metal oxide surface with a high density of O to enable the formation of more hydrogen bonds with the H(–OH) of biomolecules as an anode material target. Our study already shows that the anatase (101) surface is a very promising component of the anode nanocomposites in benthic MFCs.

Conclusions

To develop efficient and practical anode materials in mediator-less benthic MFCs, it is necessary to develop a TiO_2 with a specific biocompatible function which can be incorporated with conductive polymers as porous nanocomposites. In this work, we have demonstrated the favorable selectivity of the anatase TiO_2 (101) surface in adsorbing the common functional groups of biomolecules (carboxyl, hydroxyl, and amino in decreasing order) using the DFTB-D method. Akin to the experimental situation, our calculations considered the impact of the explicit water environment and room temperature on all possible adsorptions. Specifically, the carboxyl O formed an O-Ti bond with the surface Ti; the hydroxyl H/O formed a hydrogen bond/electrostatic attraction with the surface O/Ti; and as the ammonium group approaches the surface, the proton combines easily with the surface O then the deprotonated amino gradually moves away from the surface. A water environment to some extent elongates the O-Ti bonds and reduces the opportunity of zL-Ser/surface interactions.

Mulliken charge analysis shows that the hydrogen bond between the hydroxyl H and the surface O is an ideal pathway for electron transfer from the biomolecules to the anode surface, which is a favorable approach to increasing the output power density of MFCs. By contrast, the O-Ti bond and proton migration to the surface drive the electron transfer in the opposite direction. Fortunately, a marine environment is usually weakly alkaline, which can help avoid surface binding with protons. As a guideline and reference for future experimental work, our study suggests that the larger O density of the metal oxide surface will promote electron transfer from the biomolecules to the anode surface by forming more hydrogen bonds between them. Our study has shown that the anatase (101) surface is a promising candidate to be a component of the anode material in benthic MFCs.

Acknowledgements

The authors acknowledge the financial support of the Qingdao Applied Basic Research Programs of China (No. 12-1-4-1-(14)-jch), the Natural Science Foundation of Shangdong Province of China (ZR2011BQ018), the Hong Kong Baptist University Strategic Development Fund, and the High Performance Cluster Computing Centre,

Hong Kong Baptist University, which receives funding from the Research Grants Council, University Grants Committee of the Hong Kong Special Administrative Region, and Hong Kong Baptist University.

References

1 H. J. Kim, M. S. Hyun, I. S. Chang and B. H. Kim, *J. Microbiol. Biotechnol.*, 1999, **9**, 365–367.

2 H. J. Kim, H. S. Park, M. S. Hyun, I. S. Chang, M. Kim and B. H. Kim, A *Enzyme and Microbial Technology*, 2002, **30**, 145–152.

3 B. H. Kim, D. H. Park, P. K. Shin, I. S. Chang and H. J. Kim, *U. S. Patent*, 1999, 5976719.

4 S. K. Chaudhuri and D. R. Lovley, *Nature Biotech.*, 2003, **21**, 1229–1232.

5 K. Rabaey, G. Lissens, S. D. Siciliano and W. Verstraete, *Biotechnology Letters*, 2003, **25**, 1531–1535.

6 H. Liu, R. Ramnarayanan and B. E. Logan, *Environ. Sci. Technol.*, 2004, **38**, 2281–2285.

7 B. E. Logan, *Environ. Sci. Technol.*, 2004, **38**, 160A–167A.

8 K. Rabaey and W. Verstraete, *Trends Biotechnol.*, 2005, **23**, 291–298.

9 D. A. Lowy, L. M. Tender, J. G. Zeikus, D. H. Park and D. R. Lovley, *Biosensors and Bioelectronics*, 2006, **21**, 2058–2063.

10 C. E. Reimers, P. Girguis, H. A. Stecher III, L. M. Tender, N. Ryckelynck and P. Whailing, *Geobiology*, 2006, **4**, 123–136.

11 H. Xia and Q. Wang, *Chem. Mater.*, 2002, **14**, 2158–2165.

12 A. Dey, S. De, A. De and S. K. De, *Nanotechnology*, 2004, **15**, 1277–1283.

13 X. W. Li, G. C. Wang, X. X. Li and D. M. Lu, *Appl. Surf. Sci.*, 2004, **229**, 395–401.

14 J. C. Xu, W. M. Liu and H. L. Li, *Mater. Sci. Eng., C*, 2005, **25**, 444–447.

15 Y. Qiao, S. Bao, C. M. Li, X. Cui,; Z. Lu and J. Guo, *ACS Nano*, 2008, **2**, 113–119.

16 R. Ganesan and A. Gedanken, *Nanotechnology*, 2008, **19**, 435709 (5pp).

17 M. R. Nabid, M. Golbabaee, A. B. Moghaddam, R. Dinarvand and R. Sedghi, *Int. J. Electrochem. Sci.*, 2008, **3**, 1117–1126.

18 S. G. Pawar, S. L. Patil, M. A. Chougule, B. T. Raut, D. M. Jundale and V. B. Patil, *Archives of Applied Science Research*, 2010, **2**, 194–201.

19 H. Zhou, L. Liu, K. Yin, S. L. Liu and G. X. Li, *Electrochem. Commun.*, 2006, **8**, 1168–1172.

20 S. O. Meroueh, K. Z. Bencze, D. Hesek, M. Lee, J. F. Fisher, T. L. Stemmler and S. Mobashery, *Proceedings of the National Academy of Sciences*, 2006, **103**, 4404–4409.

21 T. K. Korhonen, E. Nurmiaho, H. Ranta and C. S. Edén, *Infection and Immunity*, 1980, **27**, 569–575.

22 H. Nakatsuji, M. Yoshimoto, Y. Umemura, S. Takagi and M. Hada, *J. Phys. Chem.*, 1996, **100**, 694–700.

23 S. Monti and T. R. Walsh, *J. Phys. Chem. C*, 2010, **114**, 22197–22206.
24 S. Yang, Y. Kim, S. Park, H. Lim and H. Lee, *J. Phys. Chem. C*, 2011, **115**, 9131–9135.
25 P-A. Garrain, D. Costa and P. Marcus, *J. Phys. Chem. C*, 2011, **115**, 719–727.
26 L. B. Wright and T. R. Walsh, *J. Phys. Chem. C*, 2012, **116**, 2933–2945.
27 K. S. Kim and M. A. Barteau, *Langmuir*, 1988, **4**, 533–543.
28 M. Schmidt and S. G. Steinmann, *Fresenius J. Anal. Chem.*, 1991, **341**, 412–415.
29 A. Vittadini, A. Selloni, F. P. Rotzinger and M. Grätzel, *J. Phys. Chem. B*, 2000, **104**, 1300–1306.
30 G. Y. Popova, T. V. Andrushkevich, Y. A. Chesalov and E. S. Stoyanov, *Kinet. Catal.*, 2000, **41**, 885–891.
31 M. Schmidt, *Arch Orthop Trauma Surg*, 2001, **121**, 403–410.
32 M. Nilsing, S. Lunell, P. Persson and L. Ojamäe, *Surf. Sci.*, 2005, **582**, 49–60.
33 X. Q. Gong, A. Selloni and A. Vittadini, *J. Phys. Chem. B*, 2006, **110**, 2804–2811.
34 S. Monti, V. Carravetta, W. Zhang and J. Yang, *J. Phys. Chem. C*, 2007, **111**, 7765–7771.
35 S. Köppen, O. Bronkalla and W. Langel, *J. Phys. Chem. C*, 2008, **112**, 13600–13606.
36 D. Szieberth, A. M. Ferrari and X. Dong, *Phys. Chem. Chem. Phys.*, 2010, **12**, 11033–11040.
37 J. Chang, S. Ju, C. Chang and H. Chen, *J. Phys. Chem. C*, 2009, **113**, 6663–6672.
38 R. Wanbayor and V. Ruangpornvisuti, *Materials Chemistry and Physics*, 2010, **124**, 720–725.
39 J. G. Chang, H. T. Chen, S. P. Ju, H. L. Chen and C. C. Hwang, *Langmuir*, 2010, **26**, 4813–4821.
40 H. Liu, X. Wang, C. Pan and K. M. Liew, *J. Phys. Chem. C*, 2012, **116**, 8044–8053.
41 M. Elstner, D. Porezag, G. Jungnickel, J. Elsner, M. Haugk, T. Frauenheim, S. Suhai and G. Seifert, *Phys. Rev. B*, 1998, **58**, 7260–7268.
42 T. Frauenheim, G. Seifert, M. Elstner, Z. Hajnal, G. Jungnickel, D. Porezag, S. Suhai and R. Scholz, *Phys. Stat. Sol. (b)*, 2000, **271**, 41–62.
43 T. Frauenheim, G. Seifert, M. Elstner, T. Niehaus, C. Köhler, M. Amkreutz, M. Sternberg, Z. Hajnal, A. Di Carlo and S. Suhai, *J. Phys.: Condens. Matter*, 2002, **14**, 3015–3047.
44 B. Aradi, B. Hourahine and T. Frauenheim, *J. Phys. Chem. A*, 2007, **111**, 5678–5684.
45 R. Luschtinetz, J. Frenzel, T. Milek and G. Seifert, *J. Phys. Chem. C*, 2009, **113**, 5730–5740.
46 M. Rapacioli, R. Barthel, T. Heine and G. Seifert, *J. Chem. Phys.*, 2007, **126**, 124103 (7 pages).
47 Y. L. Zhao, S. Köppen and T. Frauenheim, *J. Phys. Chem. C*, 2011, **115**, 9615–9621.
48 A. Domínguez, N. H. Moreira, G. Dolgonos, T. Frauenheim and A. L. da Rosa, *J. Phys. Chem. C*, 2011, **115**, 6491–6495.
49 R. Luschtinetz, J. Frenzel, T. Milek and G. Seifert, *J. Phys. Chem. C,* 2009, **113**, 5730–5740.

50 A. R. R. Neto and H. W. Leite Alves, *Phys. Status Solidi C,* 2010, **7**, 308–311.

51 W. Heckel, B. A. M. Elsner, C. Schulz and S. Müller, *J. Phys. Chem. C.*, 2014, **118,** 10771–10779.

52 A. Tilocca and A. Selloni, *J. Chem. Phys.*, 2003, **119**, 7445–7450.

53 T. H. Tran, A. Y. Nosaka and Y. Nosaka, *J. Phys. Chem. B*, 2006, **110**, 25525–25531.

54 M. Lazzeri, A. Vittadini and A. Selloni, *Phys. Rev. B*, 2001, **63**, 155409 (9 pages).

55 M. Lazzeri, A. Vittadini and A. Selloni, *Phys. Rev. B*, 2002, **65**, 119901 (1 page).

56 E. Lindahl, B. Hess and D. van der Spoel, *J. Mol. Model*, 2001, **7**, 306–317.

57 H. Lin, X. Wang and X. Fu *Progress in Chem.*, 2007, **19**, 665–670.

58 G. S. Herman, Z. Dohnálek and N. Ruzycki, *J. Phys. Chem. B*, 2003, **107**, 2788–2795.

59 A. Vittadini, A. Selloni, F. P. Rotzinger and M. Grätzel, *Phys. Rev. Lett.*, 1998, **81**, 2954–2957.

60 G. V. Samsonov, The Oxide Handbook, *IFI/Plenum Press*, New York, 1982.

61 F. Tielens, C. Gervais, J. F. Lambert, F. Mauri and D. Costa, *Chem. Mater.*, 2008, **20**, 3336–3344.

62 Y. L. Zhao, *J. Theo. & Compu. Chem.*, 2012, **11**, 155–162.

63 Z. Pan, Z. Sun, Z. Xie, J. Xu, I. Kojima and S. Wei, *J. Phys. D: Appl. Phys.* 2006, **39**, 2796–2804.

64 Y. Zhai, Y. L. Zhao, *J. Theo. & Comput. Chem.* 2013, **12**, 1350019 (12 pages).

Figure and Table Captions

Figs. 1 (a)-(e) static geometries of S1 to S5 as the L-Ser is adsorbed on the anatase (101) surface; (f)-(j) MD configurations of $S1_{vac}$ to $S5_{vac}$ at 10ps in vacuum; (k)-(o) MD configurations of $S1_{sol}$ to $S5_{sol}$ at 10ps in 163 H_2O. Silver, red, white, gray, and blue colors represent Ti, O, H, C, and N atoms, respectively.

Fig. 2 Time evolution of the distance between atoms O2 and Ti_{surf} (a) and between the H/H^+(–COOH) and atom $O1/O_{surf}$ (b) as the carboxyl/carboxylic part interacts with the surface, for different adsorption geometries (as labeled in each panel).

Fig. 3 Time evolution of the distance between atoms H(–OH) and O_{surf} (a) and between atoms O(–OH) and Ti_{surf} (b) as the hydroxyl part attaches to the surface, for different adsorption geometries (as labeled in each panel).

Fig. 4 Time evolution of the distance between atoms H(–NH_2) and O_{surf} in vacuum (a) and between atoms H^+(–NH_3^+) and O_{surf}/N in solution (b) as the amino part attaches to the surface, for different adsorption geometries (as labeled in each panel).

Table 1 Critical interatomic distances in 15 configurations displayed in Fig. 1 and in a single L-Ser and zL-Ser. Data over 3 Å are not shown.

Table 2 Adsorption energy E_{ads} and strain energy E_{strain} of neutral L-Ser attached on the anatase TiO_2 (101) surface, obtained by DFTB-D optimizations (unit: kcal/mol).

Table 3 Total energy E_{tot}, temperature T and their root mean squared deviations (RMSD) during DFTB-D/MD simulations in vacuum and solution.

Table 4 Comparison of O-Ti bond lengths and their RMSD, and O-Ti bond length differences of adsorption geometries in vacuum and solution.

Table 5 Mulliken partial charges on different parts of the adsorption systems at 10ps in vacuum and solution. (Charge unit: electron)

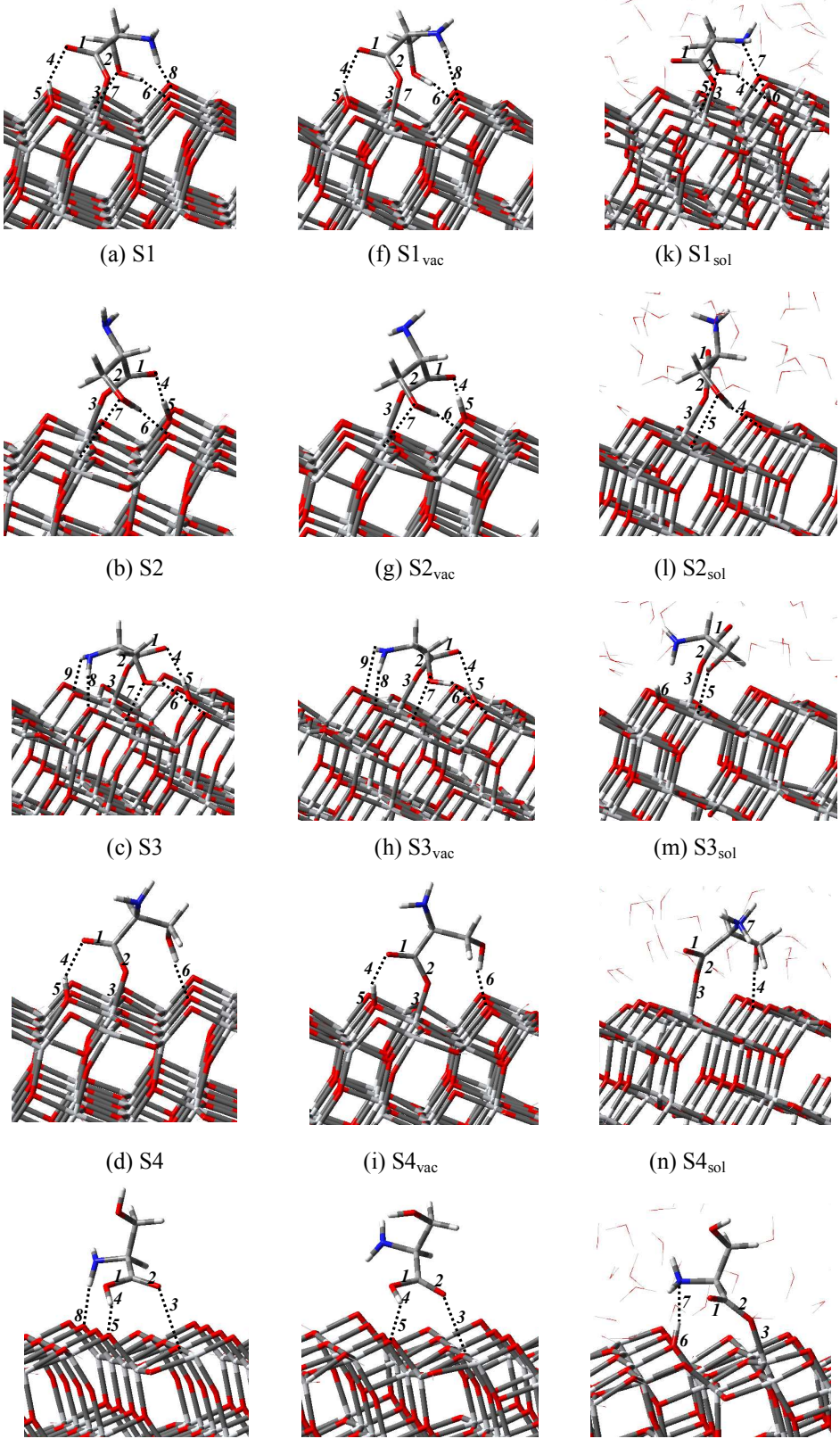

(a) S1 (f) $S1_{vac}$ (k) $S1_{sol}$

(b) S2 (g) $S2_{vac}$ (l) $S2_{sol}$

(c) S3 (h) $S3_{vac}$ (m) $S3_{sol}$

(d) S4 (i) $S4_{vac}$ (n) $S4_{sol}$

(e) S5 (j) $S5_{vac}$ (o) $S5_{sol}$

Fig.1 Zhao *et al.*

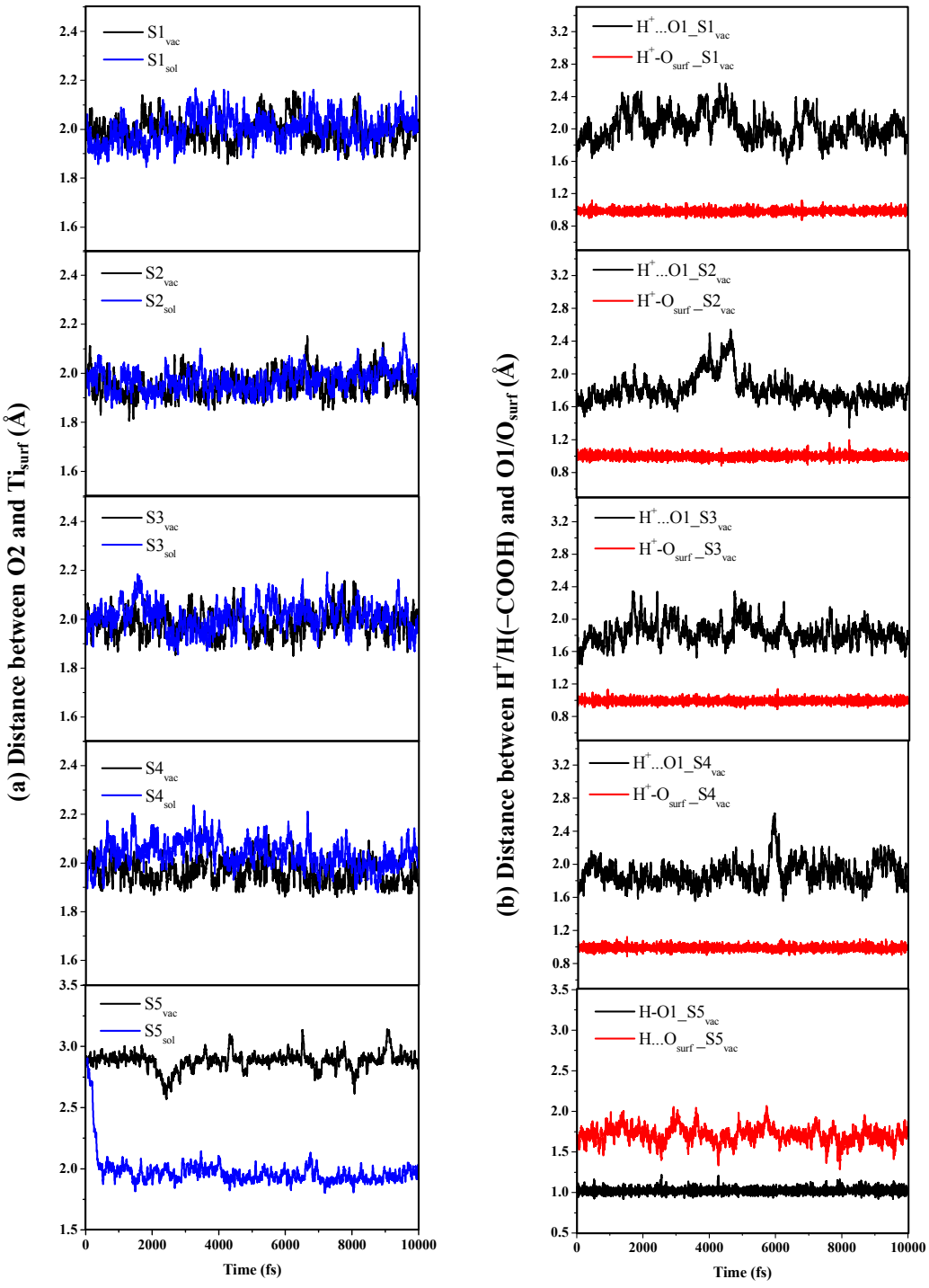

Fig.2 Zhao *et al.*

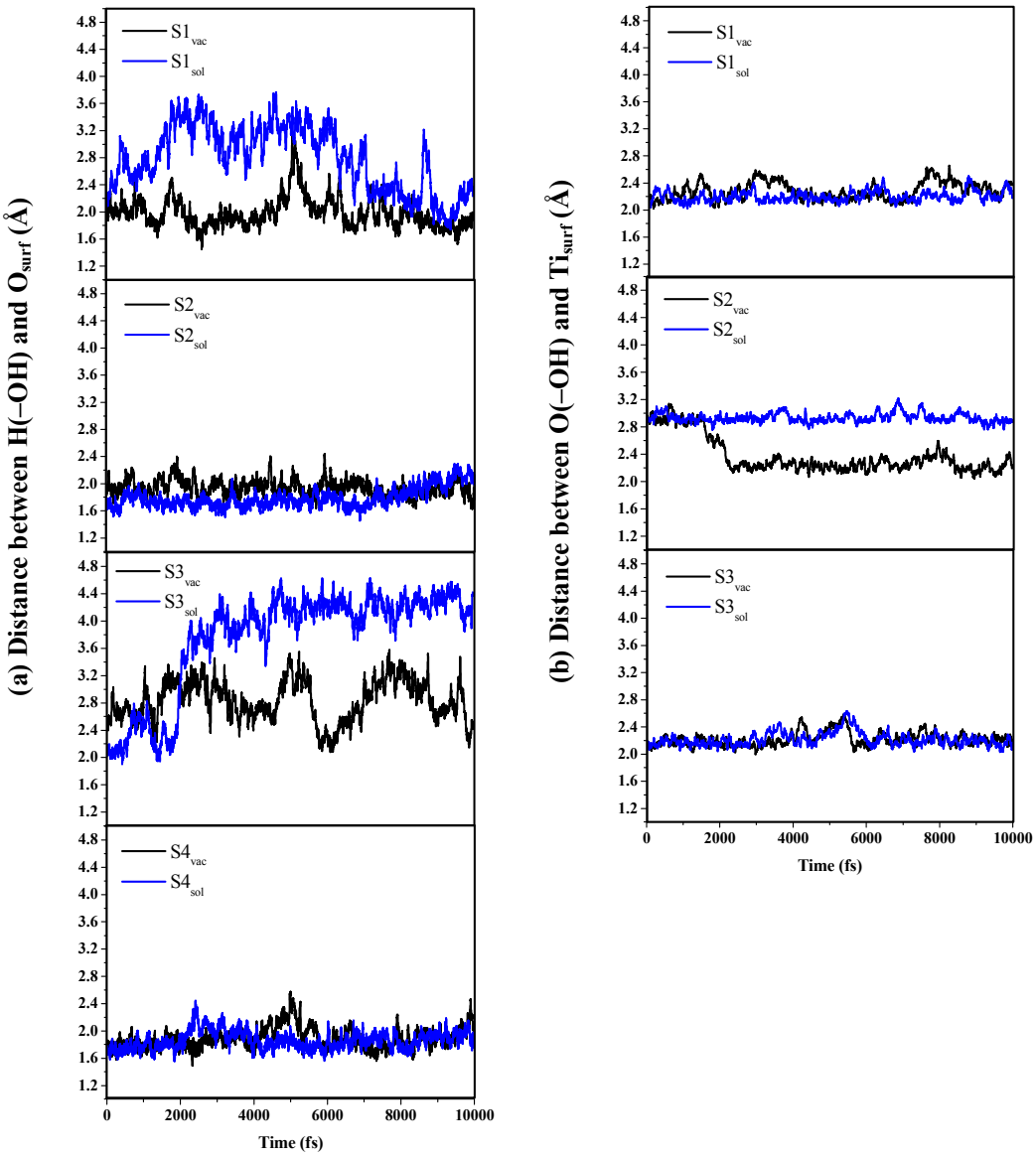

Fig.3 Zhao *et al.*

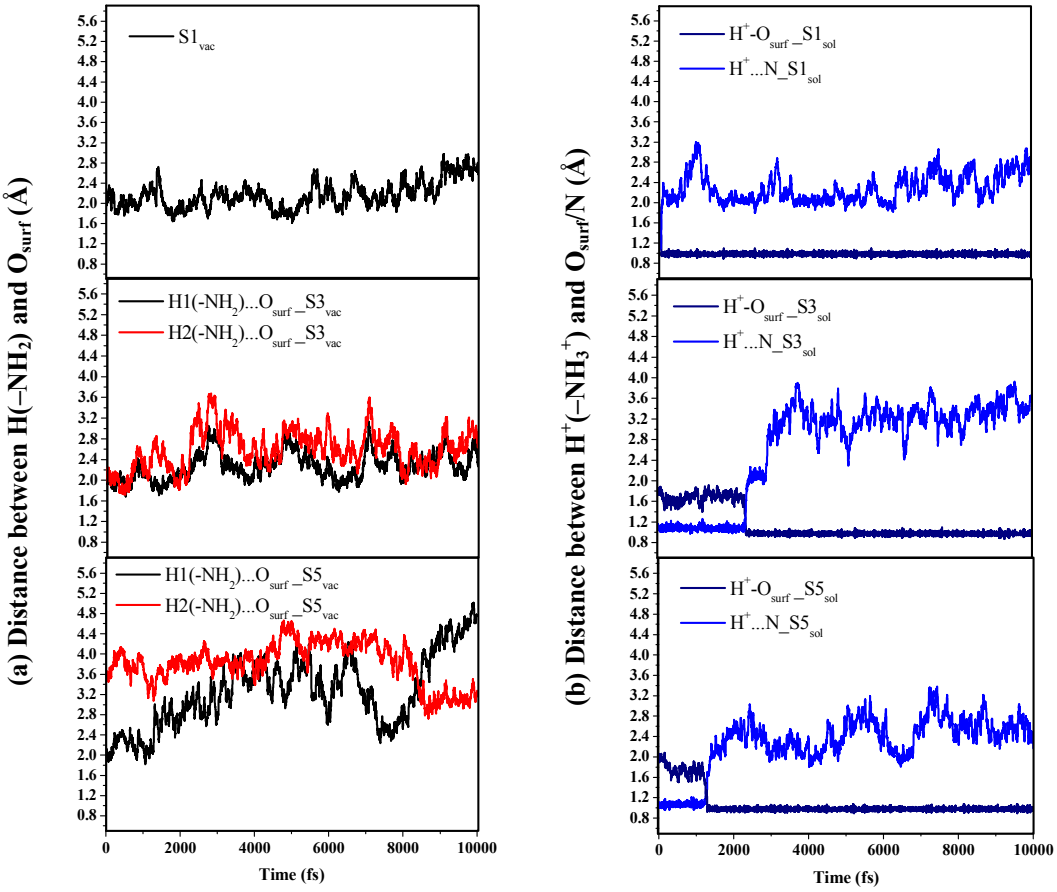

Fig.4 Zhao *et al.*

Table 1 Critical interatomic distances in 15 configurations displayed in Fig. 1 and in a single L-Ser and zL-Ser

Label	**Distances after optimizations (Å)**	**L-Ser**	**S1**	**S2**	**S3**	**S4**	**S5**
1	between carboxyl C and O1	1.380	1.245	1.253	1.253	1.248	1.347
2	between carboxyl C and O2	1.218	1.328	1.305	1.308	1.323	1.234
3	between O2 and Ti_{surf}	—	2.012	1.986	1.993	1.983	2.892
4	between H/H^+(–COOH) and O1	0.982	1.820	1.669	1.735	1.765	1.013
5	between H/H^+(–COOH) and O_{surf}	—	0.989	1.005	0.993	0.992	1.700
6	between H(–OH) and O_{surf}	—	2.010	1.858	2.442	1.758	—
7	between O(–OH) and Ti_{surf}	—	2.152	2.892	2.160	—	—
8	between H(–NH_2) and O_{surf}	—	2.008	—	1.952	—	2.042
9	between H(–NH_2) and O_{surf}	—	—	—	2.158	—	—
Label	**Distances at 10ps in vacuum (Å)**		**$S1_{vac}$**	**$S2_{vac}$**	**$S3_{vac}$**	**$S4_{vac}$**	**$S5_{vac}$**
1	between carboxyl C and O1		1.210	1.271	1.247	1.221	1.336
2	between carboxyl C and O2		1.332	1.306	1.295	1.387	1.231
3	between O2 and Ti_{surf}		2.019	1.990	2.037	1.906	2.824
4	between H/H^+ (–COOH) and O1		1.924	1.961	1.715	1.689	0.999
5	between H/H^+ (–COOH) and O_{surf}		0.969	0.975	0.983	0.981	1.877
6	between H(–OH) and O_{surf}		1.952	1.768	2.529	2.022	—
7	between O(–OH) and Ti_{surf}		2.377	2.224	2.129	—	—
8	between H(–NH_2) and O_{surf}		2.824	—	2.268	—	—
9	between H(–NH_2) and O_{surf}		—	—	2.634	—	—
Label	**Distances at 10ps in solution (Å)**	**zL-Ser**	**$S1_{sol}$**	**$S2_{sol}$**	**$S3_{sol}$**	**$S4_{sol}$**	**$S5_{sol}$**
1	between carboxyl C and O1	1.203	1.295	1.221	1.307	1.225	1.261
2	between carboxyl C and O2	1.204	1.292	1.331	1.298	1.348	1.359
3	between O2 and Ti_{surf}	—	2.012	1.991	1.991	1.997	1.950
4	between H(–OH) and O_{surf}	—	2.231	2.020	—	1.850	—
5	between O(–OH) and Ti_{surf}	—	2.174	2.878	2.173	—	—
6	between H^+ (–NH_3^+) and O_{surf}	—	0.951	—	1.017	—	0.964
7	between H^+ (–NH_3^+) and N	—	2.624	—	—	0.999	2.168

Table 2 Adsorption energy E_{ads} and strain energy E_{strain} of neutral L-Ser attached on the anatase TiO_2 (101) surface, obtained by DFTB-D optimizations (unit: kcal/mol)

Isomers	–COOH	–OH	$–NH_2$	Surface site	E_{ads}	E_{strain}
S1	Deprotonted state Hydrogen bond O-Ti bond	Hydrogen bond Coulomb attraction	Hydrogen bond	Top	-46.15	14.35
S2	Deprotonted state Hydrogen bond O-Ti bond	Hydrogen bond Coulomb attraction	—	Hollow	-43.77	11.07
S3	Deprotonted state Hydrogen bond O-Ti bond	Coulomb attraction	Hydrogen bond	Hollow	-42.18	17.30
S4	Deprotonted state Hydrogen bond O-Ti bond	Hydrogen bond	—	Top	-39.15	15.05
S5	No proton transfer Hydrogen bond	—	Hydrogen bond	Hollow	-19.71	2.07

Table 3 Total energy E_{tot}, temperature T and their root mean squared deviations (RMSD) during DFTB-D/MD simulations in vacuum and solution

Isomers	Time period	E_{tot} (kcal/mol)	RMSD (kcal/mol)	T (K)	RMSD (K)
$S1_{vac}$	7-10ps	-446871.2015	*17.087*	300.083	*14.091*
$S2_{vac}$	7-10ps	-446866.8686	*17.572*	302.062	*14.636*
$S3_{vac}$	7-10ps	-446867.2428	*16.972*	299.393	*14.313*
$S4_{vac}$	7-10ps	-446861.2790	*17.780*	300.487	*14.333*
$S5_{vac}$	7-10ps	-446845.7569	*17.641*	300.006	*14.342*
$S1_{sol}$	7-10ps	-864094.4094	*35.789*	306.455	*9.215*
$S2_{sol}$	7-10ps	-864058.9689	*28.318*	306.381	*9.357*
$S3_{sol}$	7-10ps	-864100.1290	*31.016*	306.461	*8.803*
$S4_{sol}$	7-10ps	-864059.4640	*29.863*	306.330	*8.895*
$S5_{sol}$	7-10ps	-864014.3945	*105.269*	306.984	*9.066*

Table 4 Comparison of O-Ti bond lengths and their RMSD, and O-Ti bond length differences of adsorption geometries in vacuum and solution

Time period	Isomers	$D_{O\text{-}Ti}$ (Å)	RMSD (Å)	Isomers	$D_{O\text{-}Ti}$ (Å)	RMSD (Å)	$\Delta D_{O\text{-}Ti}$ (Å)
7-10ps	$S1_{vac}$	1.980	0.053	$S1_{sol}$	2.012	0.049	0.032
7-10ps	$S2_{vac}$	1.963	0.046	$S2_{sol}$	1.995	0.045	0.032
7-10ps	$S3_{vac}$	1.998	0.051	$S3_{sol}$	2.013	0.055	0.015
7-10ps	$S4_{vac}$	1.950	0.043	$S4_{sol}$	2.007	0.046	0.057

Table 5 Mulliken partial charges on different parts of the adsorption systems at 10ps in vacuum and solution (charge unit: electron)

Name		$S1_{vac}$	$S2_{vac}$	$S3_{vac}$	$S4_{vac}$	$S5_{vac}$	$S1_{sol}$	$S2_{sol}$	$S3_{sol}$	$S4_{sol}$	$S5_{sol}$
anatase (101) surface		—	—	—	—	-0.036	-3.477	-3.858	-3.938	-3.384	-3.493
Protonated surface		+0.336	+0.302	+0.276	+0.406	—	-3.155	—	-3.637	—	-3.162
L-Ser/zL-Ser		—	—	—	—	+0.036	—	+0.337	—	+0.293	—
Deprotonated L-Ser/zL-Ser		-0.336	-0.303	-0.276	-0.407	—	-0.285	—	-0.325	—	-0.470
$163H_2O$		—	—	—	—	—	+3.440	+3.520	+3.962	+3.091	+3.632
proton		+0.340	+0.350	+0.363	+0.345	+0.367	+0.322	—	+0.301	—	+0.331
O-Ti bond	O2	-0.489	-0.471	-0.459	-0.473	-0.522	-0.463	-0.478	-0.443	-0.477	-0.485
	Ti_{surf}	+0.994	+0.907	+0.869	+0.968	+0.990	+0.895	+0.910	+0.899	+0.979	+0.963
Coulomb interaction	O(–OH)	-0.389	-0.375	-0.324	—	—	-0.309	-0.499	-0.379	—	—
	Ti_{surf}	+0.891	+0.858	+0.911	—	—	+0.887	+0.876	+0.884	—	—
Hydrogen bonding	H(–OH)	+0.356	+0.362	+0.342	—	+0.171	—	+0.358	—	+0.333	—
	O_{surf}	-0.538	-0.572	-0.520	—	-0.530	—	-0.603	—	-0.620	—

Table of content

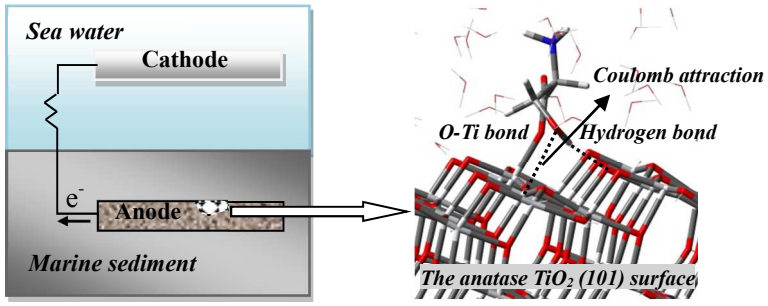

In unmediated benthic microbial fuel cells, titania anode surface as a promising candidate can have effective interactions with the carboxylic and hydroxyl groups of bacteria or pili.